

Topological transitions with continuously monitored free fermions

Graham Kells*

*Dublin City University, School of Physical Sciences, Glasnevin, Dublin 9, Ireland and
Dublin Institute for Advanced Studies, School of Theoretical Physics, 10 Burlington Rd, Dublin 4, Ireland*

Dganit Meidan

Department of Physics, Ben-Gurion University of the Negev, Beer-Sheva 84105, Israel[†]

Alessandro Romito[‡]

Department of Physics, Lancaster University, Lancaster LA1 4YB, United Kingdom

(Dated: May 5, 2022)

We study a free fermion model where two sets of non-commuting continuous measurements induce a transition between area-law entanglement scaling phases of distinct topological order. We find that, in the presence of unitary dynamics, the two topological phases are separated by a region with sub-volume scaling of the entanglement entropy and that the transition universality class of the measurement-only model differs from that in interacting models with stroboscopic dynamics and protective measurements. We further show that the phase diagram is qualitatively captured by an analytically tractable non-Hermitian Hamiltonian model obtained via post-selection. By the introduction of a partial-post-selection continuous mapping, we show that the topological distinct phases of the stochastic measurement-induced dynamics are uniquely associated with the topological indices of the non-Hermitian Hamiltonian.

I. INTRODUCTION

The complex quantum dynamics of many-body systems underpins numerous fundamental physical phenomena, from the (non-)thermalization of isolated systems [1, 2] to the information scrambling in an open quantum setting [3] and chaos in black holes [4–6]. In this context, the possibility of following individual readouts in monitored quantum circuits promises a unique platform that simultaneously generates and diagnoses complex dynamical behaviours. A prominent example is the discovery that weak measurement can both induce and diagnose entanglement scaling phase transitions [7–11].

The basic mechanism behind this transition is the quantum Zeno effect whereby frequently occurring measurements constrain the local degrees of freedom, resulting in sub-extensive entropy scaling. Several methods have used this mechanism to stabilize quantum states with distinct topological order. In [12] for example this idea is used to steer the Lindbladian dynamics of spin chains. Another approach is via quantum trajectories where dynamics is driven by projective measurements alone [13], or in combination with Clifford unitaries [14–16].

These latter works show how one can identify measurement induced topological phase transitions by tracking indicators established for ground states of gaped systems, e.g. the topological entanglement entropy [17, 18], as opposed to the explicit construction of the topological indices. Moreover, Clifford circuits do not allow for the general implementation of non-projective and continuous measurements, which are the natural ones for many experimental architectures [19–24]. Indeed, for non-projective (weak) measurements the entanglement phase transitions appear to have different universality features [11, 25–43] due to the non-linear dependence of the back-action on the state itself, which are retained in the continuum limit. Importantly, continuous monitoring can be implemented in free fermion models, and thus offer computational tractability comparable to Clifford circuits. Here, measurements can induce a transition between an area law and a critical phase with a logarithmic entanglement scaling in one-dimension [44–46], and can be obtained analytically within an effective field theory [47].

In this work we show that a topological transition can be induced in a free fermion system subjected to unitary dynamics and *continuous monitoring* of two competing observables. Taking advantage of the inherent numerical tractability and available analytical formalism, we identify two topologically distinct short range entanglement phases separated by a critical phase with a logarithmic scaling of the entanglement entropy. We show that this topological transition differs from its unitary-projective counterpart, e.g. in its finite size-scaling critical exponent. Finally, exploiting the continuous measurements setting, allows us to unambiguously associate topological invariants to the

* gkells@stp.dias.ie

† dganit@bgu.ac.il

‡ alessandro.romito@lancaster.ac.uk

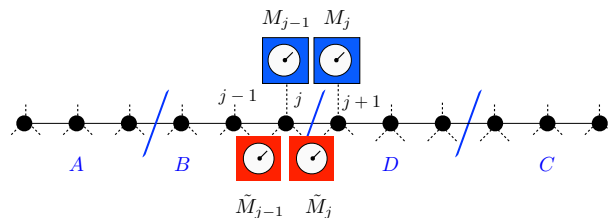


FIG. 1. Monitored system and detector model. A 1-dimensional chain of fermion hopping between next-nearest sites (gray arrows) which are monitored by local detectors sensing the local occupation M_j (upper boxes) and the occupation of the “Kitaev modes” \tilde{M}_j (lower boxes). Blue lines mark the regions A, B, D and C used to define the topological entanglement entropy in eq (4).

topological phases of the non-unitary stochastic dynamics via a partial post-selection mapping to a parent non-Hermitian Hamiltonian. Our results mark a clear distinction between the topological phase transition induced by projective and continuous measurements, and open a door to the construction of topological invariants for stochastic quantum dynamics.

II. MODEL

We study a system of fermions in a one-dimensional lattice, with sites labelled by $j = 1, \dots, L$, evolving in time under the effect of a local Hamiltonian and two sets of local continuous measurements, as sketched in Fig. 1. The corresponding dynamics is described by a stochastic Schrödinger equation [48], which takes the form of a Wiener process for the differential evolution of the system’s state, $|\psi_t\rangle$ over an infinitesimal time-step,

$$|\psi_{t+dt}\rangle = \frac{1}{\mathcal{N}} \left[1 - iHdt + \frac{1}{2} \sum_j \delta W_{j,t} M_j + \delta \tilde{W}_{j,t} \tilde{M}_j + \frac{1}{2} \sum_j \left(\gamma \langle M_j \rangle_t M_j + \alpha \langle \tilde{M}_j \rangle_t \tilde{M}_j \right) dt \right] |\psi_t\rangle. \quad (1)$$

Here H is the system’s Hamiltonian and M_j and \tilde{M}_j are the Hermitian operators associated with two non-commuting positive operator valued measures (POVM) observables at site j . The Wiener stochastic increments δW_j , $\delta \tilde{W}_j$ are independently Gaussian-distributed with $\langle \delta W_j \rangle = 0$, $\langle \delta W_j \delta W_{j'} \rangle = \gamma dt \delta_{j,j'}$ and $\langle \delta \tilde{W}_j \rangle = 0$, $\langle \delta \tilde{W}_j \delta \tilde{W}_{j'} \rangle = \alpha dt \delta_{j,j'}$. The overall constant \mathcal{N} ensures the normalisation of the state, while γ and α are the parameter controlling the strength of the two measurement sets, so that $1/\gamma$ and $1/\alpha$ set the typical time at which the system evolves close to one of the eigenstates of the measured operators, M_j and \tilde{M}_j , respectively. The process is equivalently described in terms of quantum detectors linearly coupled to M_j and \tilde{M}_j with readouts given by $x_j = \langle \psi_t | M_j | \psi_t \rangle + W_j$ and $\tilde{x}_j = \langle \psi_t | \tilde{M}_j | \psi_t \rangle + \tilde{W}_j$, as reported in Sec. II A. Note that the presence of the expectation values $\langle M_j \rangle_t = \langle \psi_t | M_j | \psi_t \rangle$ make the evolution a non-linear function of the state $|\psi_t\rangle$.

Hereafter, we specify the Hamiltonian to describe nearest neighbour hopping,

$$H = w \sum_{j=1}^{L-1} c_{j+1}^\dagger c_j + \text{h.c.}, \quad (2)$$

with c_j the fermionic annihilation operators at site j , and w the magnitude of the hopping measurement, and the measurement to two non-commuting sets of observable:

$$M_j = 2c_j^\dagger c_j - 1, \\ \tilde{M}_j = 2d_j^\dagger d_j - 1 = \left(c_{j+1}^\dagger - c_{j+1} \right) \left(c_j^\dagger + c_j \right), \quad (3)$$

where $d_j = (c_j + c_{j+1} + c_j^\dagger - c_{j+1}^\dagger)/2$ with $0 \leq j \leq L-1$. [49] assumes open boundary conditions, but can be generalised to periodic boundary conditions with $L \rightarrow L+1$ and the identification $L+1 = 1$. The operator M_j is the occupancy of site

j (relative to half-filling) and requires a detector coupling to a single chain site, while the back-action from \tilde{M}_j requires detectors coupling to pairs of adjacent sites (cf. Fig. 1). The physical meaning of the operator \tilde{M}_j can be understood by considering that the modes d_j are the eigenmodes of the Kitaev Hamiltonian for spinless p-wave superconductor [50] in the limit of single-site coherence length, $H_K = \alpha \sum_{j=1}^L (c_j^\dagger c_{j+1} + c_j^\dagger c_{j+1}^\dagger) + \text{h.c.} = 2\alpha \sum_{j=1}^{L-1} (d_j^\dagger d_j - 1/2)$. The operator \tilde{M}_j corresponds to the occupation of those modes (relative to half-filling). A possible measurement scheme for the detection of \tilde{M}_j is presented in Appendix A.

The model displays a competition between the free unitary dynamics, which generates extensive entanglement, and the local density measurements, which drive the system towards a disentangled state with a well defined site occupancy. The resulting disentanglement transition has been studied for free fermionic systems [26, 45, 47]. The key element in this work is the presence of two sets of local measurements. Competing measurement models in Bosonic systems have been shown to drive a disentanglement transition [51]. Here, due its fermionic nature, the additional "Kitaev-density", \tilde{M}_j , drives the system towards a topologically distinct disentangled state characterised by a definite occupancy of the d -modes. With the introduction of this term, the model introduces (i) a competition between two non commuting measurements that are trying to localise the system onto different short-range entangled states and (ii) the presence of a phase with short range entanglement and a topologically protected 2-fold degeneracy. Differently from previous works [14, 16], Gaussian states will remain such throughout the time evolution in our model, which will allow for an efficient numerical simulation of large-size systems.

In order to study the entanglement and topological properties of the system state, we will use a combination of the topological entanglement entropy [15, 17, 18, 52, 53] and half-cut entanglement entropy. The former is defined as

$$\bar{S}_L^{\text{top}} = \bar{S}_L^{AB} + \bar{S}_L^{BC} - \bar{S}_L^B - \bar{S}_L^{ABC}, \quad (4)$$

where $S_L^X = -\text{Tr}[\rho_X \ln \rho_X]$ is the Von Neumann entropy computed for the reduced density matrix ρ_X associated with the region X , and defined for the specific cuts configurations in Fig. 1(a). The half cut entanglement entropy is the entanglement entropy where the partial trace is taken over precisely half of the wire $\bar{S}_L^{AB} = \bar{S}_L^{CD}$ and will denoted in shorthand $\bar{S}_L \equiv \bar{S}_L^{AB}$ in what follows. Due to the stochastic nature of the system's state evolution both quantities are defined as averaged quantities over such stochastic fluctuations, and we have denoted such average by $\bar{\cdot}$ and kept explicitly the dependence on the system size L . The topological entanglement entropy is devised to be a generic indicator of topological ground states of an Hamiltonian which returns the quantum dimension of the given topological phase and it has been employed to diagnose a measurement induced topological phase transition from stroboscopic projective measurements in a stabiliser circuit model [14].

Due to the Gaussian nature of the states of the model, the half-cut and topological entanglement entropy can be computed from 2-points correlation functions $C_{ij}(t) = \langle \psi(t) | c_i^\dagger c_j | \psi(t) \rangle$ and $F_{ij} = \langle \psi(t) | c_i c_j | \psi(t) \rangle$ [34, 54, 55] as described in Sec. II section along with the procedure for the numerical simulations. We note here that the entanglement entropy is a non-linear function of the system's density matrix (and correlation matrix), so its average depends on the full distributions of states rather than the average state of the system described by the averaged density matrix.

A. Implementation of the time-evolution

We simulate numerically the time evolution of a generic initial state in Eq. (1) via quantum monte-carlo where the time evolution is determined over sufficiently small time-steps. Each of the measurement of the operators M_j can be written as $M_j = a_+ \Pi_{j,+} + a_- \Pi_{j,-}$ in terms of projectors into its eigenstates $\Pi_{j,\pm}$ and corresponding eigenvalues $a_\pm = \pm 1$. We consider the response by a one-dimensional pointer detector linearly coupled to M_j [48, 56]. The associated Kraus operator is $K_j(x, \lambda) = G(x + a_+) \Pi_{j,+} + G(x + a_-) \Pi_{j,-}$, where $G(x) = \exp(-x^2/2\lambda^2)/\pi^{1/2}$ and the parameter $\lambda^2 = \gamma dt$ quantifies the measurement backaction. For a state $|\psi_t\rangle$ the measurement outcome for the j -th operator is drawn from the distribution

$$P_j(x) = \langle \psi_t | K_j^\dagger(x, \lambda) K_j(x, \lambda) | \psi_t \rangle, \quad (5)$$

and, for a given x , the state evolves to

$$|\psi_t\rangle \rightarrow \mathcal{L}_\gamma(|\psi\rangle) = \prod_j K_j(x, \lambda) |\psi_t\rangle / \mathcal{N}_\gamma, \quad (6)$$

where, in the limit of small dt , the infinitesimal state evolution reduces to $\mathcal{L}_\gamma(|\psi_t\rangle) = (1/\mathcal{N}_\gamma) e^{-\gamma \sum_j (\langle M_j \rangle dt + \delta W_j) M_j} |\psi\rangle$ in agreement with Eq. (1). In the presence of two non-commuting measurements and Hamiltonian, the effect over an

infinitesimal step is obtained by a trotterization of the evolution operator via

$$|\psi_{t+dt}\rangle = \mathcal{L}_\gamma (\mathcal{L}_\alpha (e^{-iHdt} |\psi_t\rangle)) \quad (7)$$

where we have defined $\mathcal{L}_\alpha (|\psi\rangle) = (1/\mathcal{N}_\alpha) e^{-\alpha \sum_j (\langle \tilde{M}_j \rangle dt + \delta \tilde{W}_{j,t}) \tilde{M}_j} |\psi\rangle$. Since we are typically interested in the long-time dynamics of the system, the result would not depend on the choice of the initial state (except of the conservation of the total fermionic parity associated with the evolution in Eq. 2), which we assume hereafter to consist of an half-filling state with single fermionic occupation of odd sites in the chain.

The simulation of the stochastic process allows us to obtain the time-evolution of the full probability distribution of pure states of the system as opposed to the evolution of the averaged density matrix of the system. The former is essential to provide access to the entanglement properties of the system and its scaling, to which the average evolution is instead oblivious.

Practically speaking, as all operators are quadratic in the number of fermions but not necessarily number conserving, we implement this calculation within the BdG formalism. We represent our states as the

$$|\psi(t)\rangle = \prod_{n=1}^L \beta_n(t) |0\rangle \quad (8)$$

where the β^\dagger and β operators are encoded as a $2L \times 2L$ matrix of orthonormal vectors

$$\mathbf{W}(t) = \begin{pmatrix} U(t) & V(t)^* \\ V(t) & U(t)^* \end{pmatrix} \quad (9)$$

such that $\beta_n^\dagger = \sum_x U_{x,n} c_x^\dagger + V_{x,n} c_x$ and $\beta_n = \sum_x V_{x,n}^* c_x^\dagger + U_{x,n}^* c_x$ and $|0\rangle$ is the state with all c -fermion sites of the chain left unoccupied. We iterate the state forward in time by updating the first N columns of \mathbf{W} according to

$$\begin{pmatrix} U(t+\delta t) \\ V(t+\delta t) \end{pmatrix} = O \left(e^{\mathbf{L}_\alpha \delta t} O \left(e^{\mathbf{L}_\gamma \delta t} e^{-i\mathbf{H} \delta t} \begin{pmatrix} U(t) \\ V(t) \end{pmatrix} \right) \right) \quad (10)$$

where \mathbf{H} , \mathbf{L}_γ , and \mathbf{L}_α are $2N \times 2N$ matrices encoding the quadratic Hamiltonian and measurement operators in BdG form. The operations O represent an orthonormalisation step of the $2N \times N$ matrix implemented via Gram-Schmidt or singular value decomposition.

The representation can be used to conveniently render overlaps between different states

$$|\langle \psi_1 | \psi_2 \rangle| = |\sqrt{\det(U_1^\dagger U_2 + V_1^\dagger V_2)}|, \quad (11)$$

but more importantly for our purposes it also allows us to efficiently calculate single particle correlators

$$\mathbf{C}_{i,j}(t) = \begin{pmatrix} C_{ij}(t) & F_{ij}(t) \\ -F_{ij}^*(t) & \delta_{ij} - C_{ij}(t) \end{pmatrix} \quad (12)$$

here $C_{ij}(t) = \langle \psi(t) | c_i^\dagger c_j | \psi(t) \rangle$ and $F_{ij} = \langle \psi(t) | c_i c_j | \psi(t) \rangle$ as $C = V^* V^T$ and $F = V^* U^T$, from which we can directly calculate the entanglement entropy, see e.g. [34, 54, 55] via $S_X = -\text{Tr} [C_X \ln C_X + (1 - C_X) \ln(1 - C_X)]$.

Similarly, the entanglement entropy in the dual system is expressed in term of the d_i modes through the correlators $C'_{ij}(t) = \langle \psi(t) | d_i^\dagger d_j | \psi(t) \rangle$ and $F'_{ij}(t) = \langle \psi(t) | d_i d_j | \psi(t) \rangle$

$$S'_X = -\text{Tr} [C'_X \ln C'_X + (1 - C'_X) \ln(1 - C'_X)]. \quad (13)$$

III. RESULTS

A. Measurement-only induced topological transition

We consider first the measurement-only dynamics from the two competing non-commuting measurements by setting $w = 0$ in Eq. 2. While each of the two measurements seeks to drive the system to disentangled states associated with short range entanglement, the two phases are distinguished by the different topological properties of their steady states. This is evident by examining the statistical distribution of steady states in the limiting cases $\gamma = 0$ and $\alpha = 0$. At $\alpha = 0$, for an initial state of filling fraction n , any state of the form $|\psi\rangle_C = \prod_i p_i c_i^\dagger c_i |0\rangle$ with $p_i = 0, 1$

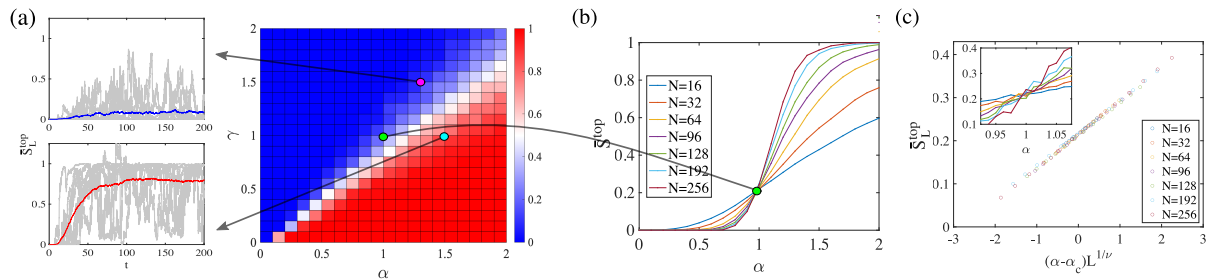


FIG. 2. Topological entanglement entropy for measurement-only dynamics ($w = 0$). (a) \bar{S}_L^{top} as a function of the two measurement strengths (α, γ). The topological entanglement entropy distinguishes the topologically trivial phases ($\bar{S}_L^{\text{top}} = 0$) from the topologically non-trivial one ($\bar{S}_L^{\text{top}} = 1$). The right panels report typical time traces of S_L^{top} (grey curves) and corresponding averages \bar{S}_L^{top} (red and blue curves) in the two regions. (b) \bar{S}_L^{top} as a function of α at constant $\gamma = 1$ for different system sizes L . The crossing point between \bar{S}_L^{top} between subsequent system sizes is used to identify the critical transition point [green dot in panel (a)]. (c) Rescaled linear fit of the data in (b) close to the transition point $\alpha = 1$ reveals precise data collapse with $\alpha_{cr} = 1 \pm O(10^{-3})$ and $\nu = 5/3 \pm O(10^{-2})$. The results are obtained for an initial state at half filling with alternating occupancies of the chain sites.

and $\sum_i p_i = n$ is a fixed point of the evolution. Similarly, in the case of $\gamma = 0$, the steady state will be drawn from a statistical distribution of states of the form $|\psi\rangle_K = \prod_i p_i d_i^\dagger d_i |0'\rangle$, where $|0'\rangle$ is now the state annihilated by the d operator. While both configurations correspond to localised short-range entangled states, the latter has a topologically protected \mathbb{Z}_2 degeneracy for open boundary conditions since all the states of the form $|\psi\rangle_K$ are eigenstates of the topologically non trivial Hamiltonian $\tilde{H} = \alpha \sum_{i=1}^L (c_i^\dagger c_{i+1} + c_i^\dagger c_{i+1}^\dagger) + \text{h.c.}$.

We report in Fig. 2 (a) typical time traces of the topological entanglement entropy for different values of the parameters, $\alpha \ll \gamma$ (right lower panel) and $\alpha \gg \gamma$ (right upper panel), respectively. After an initial transient period, S_L^{top} fluctuates around $\bar{S}_L^{\text{top}} = 0$ or $\bar{S}_L^{\text{top}} = 1$, respectively. Notably, while the trajectory-averaged entanglement entropy reaches a well defined steady state, the (topological) entanglement entropy for the individual trajectories fluctuates even in the steady state regime. This is due to the competition between the two measurements. For example, for $\alpha \gg \gamma$, while the dominant set of measurement tends to stabilise a state of the form $|\psi\rangle_K$, repeated applications of M_i measurements induce transitions between different such eigenstates (all with $S^{\text{top}} = 1$). Since these jumps occur at random times, they are averaged out in \bar{S}_L^{top} . It is also worth noting that the numerical simulations confirm that the stationary average half-cut entanglement, \bar{S}_L , does not depend on L , corresponding to an area law entangled state.

From the average steady state topological entanglement entropy \bar{S}_L^{top} , we obtain the phase diagram for the two measurement model with $w = 0$ as shown in Fig. 2 (a) for a system of size $L = 96$ with open boundary conditions. The topological entanglement entropy clearly shows the trivial and non-trivial topological phases with $\bar{S}_L^{\text{top}} = 0$ and $\bar{S}_L^{\text{top}} = 1$ respectively and a smooth crossover between the two around $\gamma \approx \alpha$. A sharp phase transition is expected in the thermodynamics limit, with two distinct area-law entangled phases characterised by $\lim_{L \rightarrow \infty} \bar{S}_L^{\text{top}} \rightarrow 0$ and $\lim_{L \rightarrow \infty} \bar{S}_L^{\text{top}} \rightarrow 1$. The transition line can be determined exactly in this instance noting that (i) after a time rescaling $t \rightarrow \gamma t$, Eq. (1) is controlled by a single parameter α/γ , and (ii) Eq. (1) is invariant under the duality transformation

$$c_j \leftrightarrow d_j, \alpha \leftrightarrow \gamma \quad (14)$$

where we have set $d_L = (c_L + c_1 + c_L^\dagger - c_1^\dagger)/2$. Consequently, the phase transition is bound to occur for $\alpha = \gamma$.

This exact result can serve a benchmark for the numerical determination of the phase transition. We can determine the phase boundary by analysing the crossing of \bar{S}_L^{top} curves at fixed γ as a function of α for different system sizes L , as shown in Fig. 2(b). The crossing points α_{cr} of curves for subsequent L values determined by $\bar{S}_L^{\text{top}}(\alpha_{cr}) = \bar{S}_{L'}^{\text{top}}(\alpha_{cr})$, converge to a finite value for increasing system size. Extrapolating the value of α_{cr} to $L \rightarrow \infty$, we determine the critical value $\alpha_{cr} \sim \gamma$, in agreement with what one expects from duality.

The numerical analysis allows further characterisation of the universality of the transition by evaluating its finite size scaling universal exponent. For this goal, the critical value $\alpha_{cr} = \gamma$ is used to rescale the data in the vicinity of the transition point according to:

$$\bar{S}^{\text{top}}(\alpha, L) = F((\alpha - \alpha_{cr})L^{1/\nu}), \quad (15)$$

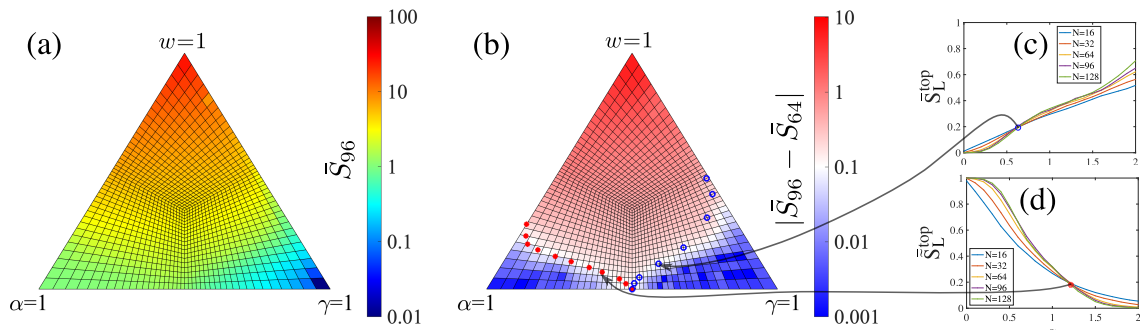


FIG. 3. Phase diagram for $w \neq 0$. (a) Density plot of \bar{S}_L as a function of w , γ and α ($w + \gamma + \alpha = 1$) in barycentric coordinates for $L = 96$. Area law scaling is recovered in the limits $\alpha = 1$ and $\gamma = 1$ with $\bar{S}_{96} = 1$ and $\bar{S}_{96} = 0$ respectively, while $w = 1$ displays volume-law scaling. (b) $\bar{S}_{96} - \bar{S}_{64}$. The entanglement entropy difference shows a sharp crossover between the three distinct phases. Transition points between the sub-volume-scaling and trivial area-law scaling (blue dots) and between the sub-volume-scaling and topological area-law scaling are determined by (c) the crossing of \bar{S}_L^{top} in c -fermion basis for fixed $w = 0.2$ and $\gamma = 0.5$ (d) \bar{S}_L^{top} in d -fermion basis (red-stars) according to (14).

where ν is used as a fitting parameter. The inset of Fig. 2 (c) shows the raw data in the vicinity of the transition for different L . This dependence is well approximated by a linear behaviour. Rescaling of the linear fits to the raw data in the vicinity of the transition is shown in Fig. 2 (b), where the data collapse is achieved with $\nu = 5/3 \pm O(10^{-2})$. The value of ν differs from the scaling of a topological phase transition from projective measurements in stabilizer circuits [14], highlighting the difference between continuous and stroboscopic models [25].

B. Dynamics under unitary evolution and competing measurements

In the presence of unitary dynamics, i.e. $w \neq 0$, the phase diagram is more intricate and exhibits in addition to the two topologically distinct disentangled states, the appearance of a critical phase with long range entanglement scaling like $\log L$. This is illustrated in Fig. 3 (a), where the limiting cases of trivial area-law scaling ($\gamma = 1$), topological area-law scaling ($\alpha = 1$), and volume-law scaling ($w = 1$) are marked by $\bar{S}_L \approx 0$, $\bar{S}_L \approx 1$ and $\bar{S}_L \gg 1$. In order to highlight the approximate transition between states with different entanglement properties we plot the difference between the entanglement half cuts obtained for different system sizes, as a function of the system parameters in Fig. 3 (b). Regions of phase space associated with short range entanglement with weak dependence on system size L and would thus appear as dark blue. This plot therefore allows to identify approximately where the transition to a system size dependent entanglement behaviour occurs.

In order to identify the phase boundaries in the thermodynamic limit, we can use the same approach used for the measurement-only dynamics based on the analysis of the crossings of \bar{S}_L^{top} for different system sizes. The corresponding critical points (marked in blue dots) are shown in Fig. 3(b), and the analysis of the crossing is reported for one instance in panel (c), which clearly detects the transition between a topologically trivial area law phases and a phase characterised by size-dependent scaling of the entropy. However, unlike the case of interacting systems [15] the numerical data do not allow to identify a transition point between the sub-volume law phase and the topological area-law phase, due to the weak sub-volume dependence on system size and the finite fixed value of the entanglement entropy in the topologically non trivial phase.

To overcome this difficulty, we take advantage of the duality transformation in (14) and treat the d_i operators as the physical fermions of the system. We implement this change of basis by performing the transformation $\gamma \leftrightarrow \alpha$ in Eq. (1). The dynamics is still described by Eq. (1), where the Hermitian Hamiltonian is replaced by its corresponding form in the d basis, $H \rightarrow H' = \frac{w}{2} \sum_i d_{i+1}^\dagger d_{i-1} + d_{i+1}^\dagger d_{i-1}^\dagger + 2d_i^\dagger d_i - 1 + \text{h.c.}$. This allows us to define the entanglement entropy of the dual system, S'_X defined as S_X with the replacement $c_i \rightarrow d_i$ (Cf. Sec. II). In the dual model, the topological non-trivial phase, characterised by a given set of occupation numbers $\langle d_i^\dagger d_i \rangle \in \{0, 1\}$ is local in this basis, and is not associated with dangling Majorana bonds. The resulting phase is identified as topologically trivial $\bar{S}^{\text{top}} = 0$. Conversely the topological trivial phase associated with a set of $\langle c_i^\dagger c_i \rangle \in \{0, 1\}$, now has $\bar{S}^{\text{top}} = 1$. The crossing of \bar{S}^{top} for different system sizes are shown in Fig. 3(d) and the critical values obtained are marked in red dot in panel (b).

These results indicate the presence of three distinct phases, two of which are characterised by an area law scaling

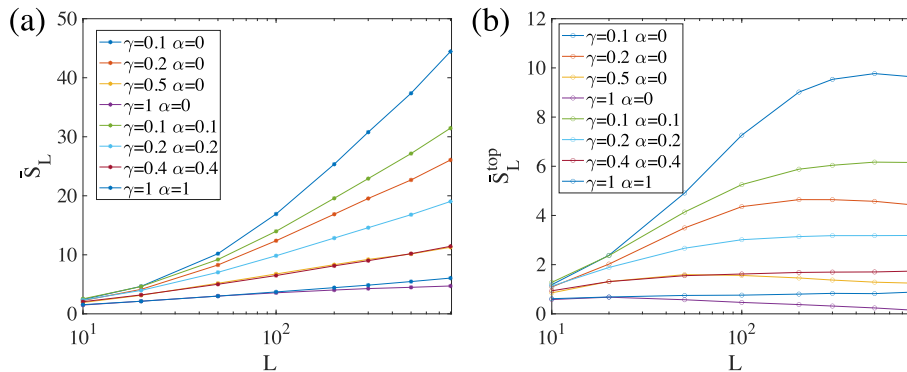


FIG. 4. System size scaling of the averaged (a) Half-cut entanglement entropy (b) Topological entanglement entropy

of the entanglement entropy and by a vanishing \bar{S}_L^{top} or \tilde{S}_L^{top} . Consequently, they can be identified with a topologically trivial and non-trivial phases, respectively. The intermediate region is distinguished via critical scaling of the entanglement entropy as shown in Fig. 4, and is not associated with topological properties. The phase boundary determined by analysing crossing points in the topological entanglement entropy \bar{S}_L^{top} and \tilde{S}_L^{top} are in agreement with the onset of entanglement growth with increasing systems size, marked as red regions in the density plot in Fig. 3. The phase space is qualitatively similar to the one obtained in related systems with stroboscopic-projective dynamics. In particular a tri-critical point is present at the dual point with vanishing unitary dynamics. [15], which is not generically observed in all measurement only models [16]. The main difference is the presence of a critical scaling region instead of a volume law one.

The scaling of the entanglement entropy, \bar{S}_L , with system size, indicates that the critical region extend to $\alpha \rightarrow 0$ with a critical value $0.5 < \gamma_c/w < 0.6$, see Fig. 4 (a). Conversely, the topological entanglement entropy \tilde{S}_L^{top} suffers from large finite size effects, due to the large system sizes required to reach the thermodynamic limit for small γ , as shown in Fig. 4(b) making it hard to identify a critical value.

C. From measured to post-selected non-Hermitian dynamics

The topological transition in the model originates from the competing stationary states stabilised by the Zeno effects of the two non-commuting measurements [16]. In order to capture this effect, it is possible to analyse sequences of predetermined measurements readouts, that stabilises one of the possible measurement eigenstates, i.e. a post-selected dynamics, which has been shown to capture area-to-volume law transitions [26, 34, 37]. In our model, we can extend this correspondence to the topological transition and show that the area law phases characterised by different topological orders are continuously connected to distinct topological phases of the non-Hermitian system. There it is possible to explicitly construct topological invariants that distinguish the different phases, see e.g. [57, 58].

The process can be readily described in terms of detector outcome $x_j = \langle \psi_t | M_j | \psi_t \rangle + W_j$. For the case of a the local density measurement, for example, it would correspond to selecting the outcome $x_j = 1$. The result is a deterministic evolution of the system via a non-Hermitian Hamiltonian (cf. Sec. II)

$$\mathcal{H} = H_0 - i\gamma \sum_{i=1}^L M_i - i\alpha \sum_{i=1}^{L-1} \tilde{M}_i \quad (16)$$

where H_0 is the Hermitian Hamiltonian in (2) and the measurements operators are defined in Eq. (3). The corresponding post-selected dynamics can be studied analytically by considering the time evolution of the quantum state $|\psi(t)\rangle = \frac{\mathcal{U}(t)}{\sqrt{Z}} |\psi(t=0)\rangle$ governed by the non-unitary evolution operator $\mathcal{U}(t) = \prod_{dt=1}^{\text{Int}[t/dt]} \exp(-idt\mathcal{H})$ followed by a normalization of the wave function $Z = \langle \psi(t) | \psi(t) \rangle$ [34].

Under the evolution $\mathcal{U}(t)$ the state $|\psi(t)\rangle$ remains Gaussian at all times. Consequently the entanglement is entirely expressed through the correlation matrix (12). We derive and solve the equations of motions for the correlation matrix $C_{i,j}(t)$ [34, 54, 55], see Appendix B.

Under the post selected dynamics, the quantum state evolves to the dark state of the effective Hamiltonian (16) $\mathcal{H} = -i\mathcal{K}$, which, in turn, is identified with the ground state of \mathcal{K} . Explicitly, $\mathcal{K} = \sum_k \Psi_k^\dagger \mathcal{K}_{BdG}(k) \Psi_k$, where $\Psi_k =$

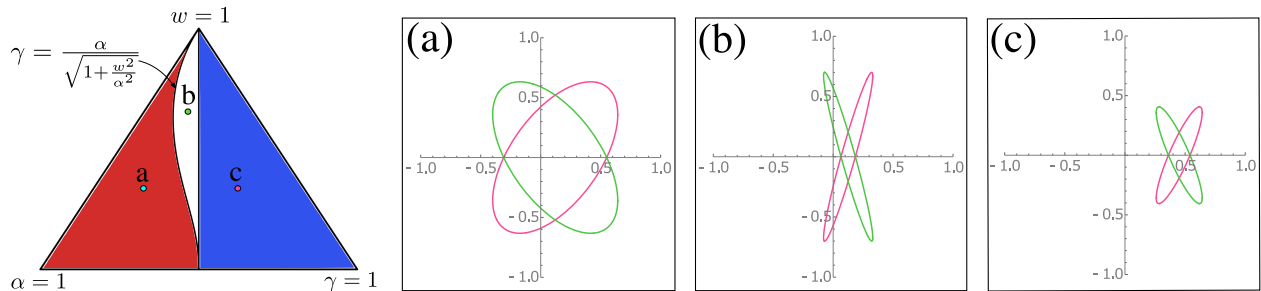


FIG. 5. The phase diagram of the effective non Hermitian model. Here blue marks a gapped topologically trivial phase with $\nu_{1,2} = 0$, red marks a gapped topologically non trivial regime $\nu_{1,2} = 1$ and white marks a gapless phase. The insets (a)-(c) show the winding of $q_1(k)$ (green curve) and $q_2(k)$ (red curve) around the origin in the gapless, topological and trivial phases, respectively.

$(c_k, c_{-k}^\dagger)^T$ and the corresponding BdG Hamiltonian is:

$$\mathcal{K}_{BdG}(k) = (\xi(k) + iw(k)) \tau_z + \Delta(k) \tau_y, \quad (17)$$

where $\xi(k) = \alpha \cos k + \gamma$, $\Delta(k) = \alpha \sin k$ and $w(k) = w \cos k$.

Eq. (17) shows that $\mathcal{K}_{BdG}(k)$ coincides with the Kitaev chain with non Hermitian hopping. Besides charge conjugation symmetry, this model possesses a chiral symmetry which can be made apparent by rotating to the chiral basis by the unitary transformation $\mathcal{R} = i\tau_y$:

$$\mathcal{K}_{BdG}^{\text{chiral}}(k) = \begin{pmatrix} 0 & q_1(k) \\ q_2(k) & 0 \end{pmatrix}, \quad (18)$$

where

$$q_{1,2}(k) = \xi(k) + i [w(k) \pm \Delta(k)] \quad (19)$$

In the Hermitian limit $w = 0$, $q_1(k) = q_2(k)^*$ and the complex vector $q_1(k) = \gamma + \alpha e^{-ik}$ marks a circle of radius α centred around γ and the topological phases are discriminated by whether the resulting circle encloses the origin, with a topological phase transition at $\alpha = \gamma$. Thus, the entanglement properties of the measurement-only model in Fig. 2 can be understood from the evolution of the corresponding post-selected quantum state to a trivial ($\gamma > \alpha$) or a symmetry protected topological ($\gamma < \alpha$) dark state in the post-selected dynamics. We note that the agreement in the transition point between the full measurement and the post-selected models is non typical, and follows from the model's self duality (14) that uniquely fixes the transition point. Therefore we expect that while both models capture the same qualitative physics, and hence show the same transition, there will be quantitative differences between them. This will become evident in the presence of the unitary dynamics $w \neq 0$, which violates the duality.

In the presence of unitary dynamics $w \neq 0$, the two complex vectors mark two tilted ellipses. Whether these ellipses encapsulate the origin determine the topological phases as shown in Fig. 5. The phase diagram of the effective non-Hermitian model exhibits three distinct phases: two gapped phases and one gapless phase. The gapped phases, corresponding to trivial and non trivial Hermitian phases, are distinguished by the winding of none ($\nu_{1,2} = 0$) or both ($\nu_{1,2} = 1$) of the complex vectors $q_{1,2}(k)$, respectively. In the gapless regime there is no winding of the complex vectors $q_{1,2}(k)$ – see Appendix B for a full analysis of the model and its properties.

The transition lines between the two distinct gapped phases and the gapless phase of the non-Hermitian model which governs the post-selected dynamics are marked as solid black line in Fig. 6, where they can be compared with the transitions obtained from the numerical analysis of the full stochastic dynamics.

The post-selected dynamics captures some of the key qualitative features of the stochastic dynamics. In particular, the presence of three distinct phases corresponding to topologically trivial and non-trivial short entanglement phases as well as the presence of a finite size region characterised by critical scaling $\propto \log L$ of both $\bar{S}_{L/2}$ and \bar{S}_L^{top} . Yet, some features are missed by the post-selected evolution. In particular the stochastic dynamics exhibits a transition from an area-law to a critical sub-volume-law scaling of the entanglement entropy at a finite critical value of γ/w in the limit of $\alpha = 0$. The post-selected dynamics, instead, produces area-law scaling for any $\gamma \neq 0$ at $\alpha = 0$ [45].

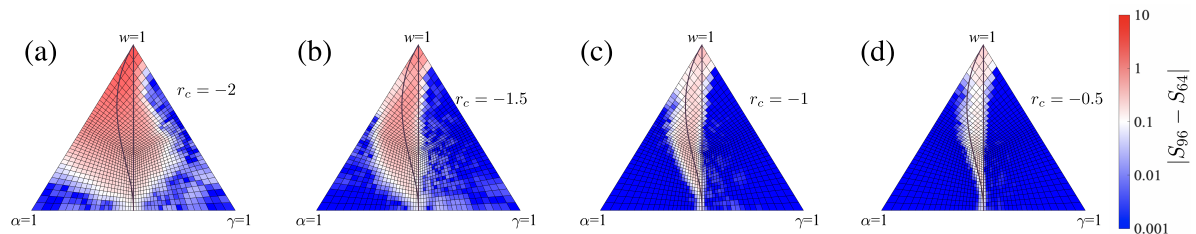


FIG. 6. Density plot of $|\bar{S}_{96} - \bar{S}_{64}|$ in the partially post-selected model in Eq. (20) with (a) $r_c = -2$, (b) $r_c = -1.5$, (c) $r_c = -1$, (d) $r_c = -0.5$. Full black lines correspond to the phase boundaries obtained from non-Hermitian dynamics (cf. Eq. (17)). The distinct phases of trivial area-law, topological area-law, and volume-law scaling are continuously deformed from the full measurement limit (a) to the strongly post-selected limit (b). The phase boundaries from the sharp crossover of $\bar{S}_{96} - \bar{S}_{64}$ agree well with the analytical predictions in the limit of strong post-selection [cf. panel (c)]

D. Interpolation between post-selected and stochastic dynamics

The qualitative similarity between the stochastic and post-selected dynamics can be understood by continuously interpolating between the two regimes. To achieve this, we take advantage of our continuous readout detector and introduce a new *partial-post-selection* measurement scheme where we include the measurement-induced stochastic fluctuations with a gradual weight beyond the deterministic non-Hermitian dynamics. The idea is to retain only a subset of the readout data.

For clarity, we discuss this procedure for the case of $\alpha = 0$ below. The generic case for $\alpha \neq 0$ readily follows. We consider the detector's readout $x_j = \langle \psi_t | M_j | \psi_t \rangle + \xi_j(t)$, with its corresponding probability distribution, $P(x)$, as discussed in Sec. II A. We modify the measurement procedure by post-selecting the measurement outcome x , so that we retain only values such that $x \geq r_c$ and discard any value for which $x < r_c$, where $r_c \in \mathbb{R}$ is a parameter that controls the degree of our post-selection. This procedure amounts to replacing the probability distribution (5) with

$$P_{r_c}(x) = \begin{cases} 0 & \text{if } x < r_c \\ P(x) & \text{if } x > r_c \end{cases}. \quad (20)$$

For $r_c \ll -1$, $P_{r_c}(x) \approx P(x)$ and the model reproduces the fully stochastic (non post-selected dynamics). In the opposite limit, $r_c \gg 1$, as long as the readout x is retained (post-selected), the corresponding dynamics is controlled by small fluctuations on top of the deterministic evolution dictated by the non-Hermitian Hamiltonian $\mathcal{H}_\gamma = -i\gamma \sum_{j=1}^L M_j$.

For intermediate values of r_c the model continuously bridges between fully stochastic and fully post-selected dynamics. The results are presented in Fig. 6 for several values of r_c . The phase diagram agrees well with the post-selected non-Hermitian dynamics already for $r_c < 0$ [cf. Fig. 6(c)] for which the update of $\langle \Pi_{+,j} \rangle$ is exponentially suppressed compared to $\langle \Pi_{-,j} \rangle$, having introduced $\Pi_{j,+} = c_j^\dagger c_j$ and $\Pi_{j,-} = 1 - c_j^\dagger c_j$ as the projectors onto the occupied and unoccupied j -th site. For $r_c < 0$, as the bias between $\langle \Pi_{+,j} \rangle$ and $\langle \Pi_{-,j} \rangle$ from the stochastic infinitesimal update starts to fade off, the approximation in terms of the post-selected dynamics breaks down. Yet, the phase diagram continuously interpolates between that induced by post-selected evolution to the fully stochastic dynamics as we change r_c . In particular, already at finite values of r_c the steady state exhibits a transition between an area-law and a critical scaling region at a *finite* critical value of γ/w , see Fig. 6 (d).

IV. DISCUSSION

We studied the stochastic evolution of a quantum state under free unitary dynamics disrupted by the back-action of two competing continuous measurements. We analysed the steady-state entanglement properties of the system, based on the behaviour of the entanglement entropy and the topological entanglement entropy.

In the absence of the unitary dynamics, the steady state of the system shows a transition between two area-law entanglement scaling phases distinguished by the presence or absence of a (symmetry-protected) topological order. While the transition point is exactly determined by the symmetries of the model, we show from numerical analysis that the universal exponent of the finite size scaling differs from its analog for stroboscopic dynamics with projective measurements. In the presence of unitary dynamics, a phase characterised by sub-volume scaling of the entanglement entropy separates the topologically distinct area-law phases. Finally, we introduce a *partial* post-selection measurement

scheme, which allows us to unambiguously connect the three phases of the weakly monitored system to those of a parent post-selected non-Hermitian Hamiltonian and, in turn, to its topological indices based on winding numbers.

The prediction of measurement-induced topological transitions in free fermionic systems provides us with a new platform for studying topological ordered phases. The connection we establish between stochastic evolution and non-Hermitian Hamiltonians is a first step towards a topological classification of non-unitary quantum stochastic dynamics.

ACKNOWLEDGMENTS

We would like to thank I. Jubb, L. Coopmans, H. Schomerus, M. Szyniszewski and Jonathan Ruhman for useful discussions. A.R. acknowledges the EPSRC via Grant No. EP/P010180/1. G.K. acknowledges the support of a DIAS Schrödinger Fellowship and the SFI Career Development Award 15/CDA/3240. D.M. acknowledges support from the Israel science foundation (grant No. 1884/18).

Appendix A: Physical implementation of the measurements operations

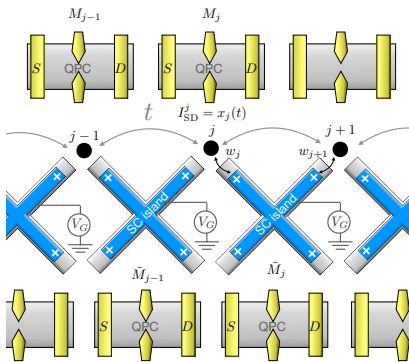


FIG. 7. Detection scheme for the operator \tilde{M}_j based on a Coulomb-blockade superconducting island (blue) hosting 4-Majorana zero modes (white). The fermionic chain can be realized i.e. by an array of tunnel coupled quantum dots. Two Majorana zero modes are tunnel coupled to adjacent chain sites, while the parity of the remaining two Majorana modes is read by a charge sensing detector.

We present here a possible measurement protocol to detect the operators \tilde{M}_j introduced in Eq. (3). The measurement protocol is based on a Majorana-island setup. While the local density M_j can be monitored via detector coupled to the system via a density-density interaction, as in commonly used charge sensors for electronic nanodevices [59, 60]), the operator \tilde{M}_j requires a modification of the system's particle number. At a formal level, \tilde{M}_j is a measurable operator since it is Hermitian, but it requires a careful design of the detector's coupling due to its structure in the particle-hole space.

If the system is realized as a chain of Majorana modes (e.g. at the edges of quasi-one-dimensional systems [61], the measurements of both M_j and \tilde{M}_j can be implemented by weak parity measurements of pairs of Majorana modes therein [62–65]. A possible detection scheme for the operator \tilde{M}_j in a system where only fermionic modes (as opposed to Majorana modes) are accessible is sketched in Fig. A.

The detector, coupled to two adjacent sites j and $j+1$, consists of an isolated superconducting island hosting 4 Majorana zero modes, η_α^j , $\alpha = 1, \dots, 4$. The superconductor is in a coulomb blockade regime where the charging energy is adjusted so that the total parity of the island is odd [66–69]. For an island hosting 4 Majorana zero modes, this results in a 2-fold degenerate space spanned by $|0, 1\rangle$ and $|1, 0\rangle$. Here $|1, 0\rangle = (\eta_1 - i\eta_2)/2 |0, 0\rangle$ and $|0, 1\rangle = (\eta_3 - i\eta_4)/2 |0, 0\rangle$ with $|0, 0\rangle$ defined by $(\eta_1 + i\eta_2) |0, 0\rangle = 0$, $(\eta_3 + i\eta_4) |0, 0\rangle = 0$. When the detector is tunnel-coupled to the system as indicated in Fig. fig:system(b), single electron tunneling will be prohibited by Coulomb blockade, and correlated electron hopping is the only term allowed, as described by the Hamiltonian

$$H_{\text{det}} = i\tilde{t}_j \eta_1^j \eta_2^j (c_j + c_j^\dagger)(c_{j+1} - c_{j+1}^\dagger) = i\tilde{t}_j \eta_1^j \eta_2^j \tilde{M}_j. \quad (\text{A1})$$

Note that the specific combination $c_j \pm c_j^\dagger$ entering the coupling of two adjacent detectors is important, and can be adjusted by controlling the flux between adjacent detectors. We further assume that the parity of pairs of Majorana

zero modes in the detector can be continuously measured, e.g. via recently proposed protocols [62–65]. Specifically we assume to perform a continuous readout of the the parity of the pairs of Majorana zero modes $\eta_{3,j}$ and $\eta_{4,j}$. The latter returns a continuous output x with probability $P(x) = \langle \Psi | \mathcal{C}^\dagger(x) \mathcal{C}(x) | \Psi \rangle$ and an associated conditional back-action

$$|\Psi\rangle \rightarrow \frac{1}{\sqrt{P(x)}} \mathcal{C}(x) |\Psi\rangle, \quad (\text{A2})$$

where

$$\begin{aligned} \mathcal{C} = & \pi^{-1/2} \left[\exp\left(-\frac{(x+\lambda)^2}{2}\right) |0,1\rangle \langle 0,1| \right. \\ & \left. + \exp\left(-\frac{(x-\lambda)^2}{2}\right) |0,1\rangle \langle 0,1| \right]. \end{aligned} \quad (\text{A3})$$

With this setup at hands, the proposed measurement protocol for the detection of \tilde{M} , consists of (i) initializing the superconducting island in a state $|\chi\rangle = [|0,1\rangle + |1,0\rangle]/\sqrt{2}$, (ii) coupling the detectors to the chain for a short time and (iii) measure the parity of the pairs of Majorana zero modes $\eta_{3,j}$ and $\eta_{4,j}$.

To show the validity of the protocol, we consider its application to the chain in a given state $|\psi\rangle$. After step (ii) above, the resulting (system-detector entangled) state is

$$\begin{aligned} |\Psi\rangle &= |\psi\rangle |\chi\rangle + g\tilde{M}_j |\psi\rangle \eta_{i,j} \eta_{2,j} |\chi\rangle \\ &= \left(1 - g\tilde{M}_j\right) |\psi\rangle |0,1\rangle + \left(1 + g\tilde{M}_j\right) |\psi\rangle |1,0\rangle \end{aligned} \quad (\text{A4})$$

to leading order in the system-detector coupling, where g is a small parameter controlled by the strength and time-duration of the system-detector coupling. Finally, the state after (iv) is computed applying Eq. (A2) to the state in Eq. (A4), and the resulting state of the chain, conditional to the measurement outcome x for small λ , takes the desired form of Eq. 6 with $\tilde{M}_j = (d_j^\dagger d_j - 1)/2$. Note that the protocol is not sensitive to fine tuning of the parameters as long as the detectors is initialized in a superposition of parity states and the system-detector coupling evolution is weak.

Appendix B: Post selected dynamics and the corresponding non-Hermitian Hamiltonian

The topological transition in the model originates from the competing stationary states stabilized by the Zeno effects of the two measurements. In order to capture this effect, it is possible to analyze individual measurements readouts, that stabilize one of the possible measurements eigenstates. The process can be readily described in terms of detector outcome. For the case of a the local density measurement, for example, it would correspond to selecting the outcome $x = a_+$ from the probability distribution in Eq. 5. The result is a deterministic evolution of the system via a non-Hermitian Hamiltonian $\mathcal{H}_\gamma = -i\gamma \sum_i M_i$. We can therefore analyze the steady state of the deterministic process determined by the overall non-Hermitian Hamiltonian

$$\mathcal{H} = H_0 - i\gamma dt \sum_{i=1}^L M_i - i\alpha dt \sum_{i=1}^{L-1} \tilde{M}_i. \quad (\text{B1})$$

The corresponding post selected model can be studied analytically following Ref 34. We consider non unitary dynamics with a time evolution operator:

$$U(t) = \prod_{t=1}^N U_1(t) U_2(t) \quad (\text{B2})$$

Where the time evolution of the post selected quantum state is governed by $U_1(t) = \exp(-\tau H_{nh})$ followed by a normalization of the wave function, where

$$H_{nh} = \frac{\alpha}{2} \sum_i \left(c_i^\dagger - c_i \right) \left(c_{i+1}^\dagger + c_{i+1} \right) + \gamma \sum_i c_i^\dagger c_i \quad (\text{B3})$$

and the unitary dynamics is modeled by a Hermitian hopping Hamiltonian $U_2(t) = \exp(-i\tau H_h)$

$$H_h = \sum_i w c_i^\dagger c_{i+1} \quad (\text{B4})$$

the wave function dynamics is given by:

$$|\psi(T)\rangle = \frac{U(T)}{\sqrt{Z}} |\psi_0\rangle \quad (\text{B5})$$

where the normalization is $Z = \langle \psi_0 | U(T)^\dagger U(T) | \psi_0 \rangle$. Under the evolution $U(T)$ the state $|\psi(T)\rangle$ remains Gaussian. Consequently the entanglement is entirely expressed through the correlation matrix:

$$\begin{pmatrix} C_{ij}(T) & F_{ij}(T) \\ -F_{ij}^*(T) & \delta_{ij} - C_{ij}(T) \end{pmatrix} \quad (\text{B6})$$

$$\begin{aligned} C_{ij}(T) &= \langle \psi(T) | c_i^\dagger c_j | \psi(T) \rangle \\ F_{ij}(T) &= \langle \psi(T) | c_i c_j | \psi(T) \rangle \end{aligned} \quad (\text{B7})$$

following 34 we derive the time evolution of the correlation matrix. The resulting equations reads:

$$\begin{aligned} \frac{dC_k}{dt} &= -4\xi(k) [C_k(1 - C_k) + |F_k|^2] \\ &\quad - i2\Delta(k)(2C_k - 1)(F_k - F_k^*) \\ \frac{dF_k}{dt} &= -4\xi(k) [F_k(1 - 2C_k)] - i4w(k)F_k \\ &\quad - 2i\Delta(k)(2F_k^2 + 2C_k^2 - 2C_k + 1) \end{aligned} \quad (\text{B8})$$

where $\xi(k) = (\alpha \cos k + \gamma)$ and $\Delta(k) = \alpha \sin k$ and $w(k) = w \cos k$. We first consider the simplified two measurement model setting $t = 0$. We seek a steady state solution. We find the following solutions:

$$\begin{aligned} F_k &= \frac{i\Delta(k)}{2\sqrt{\xi(k)^2 + \Delta(k)^2}} = \frac{i\Delta(k)}{2E(k)} \\ C_k &= \frac{1}{2} - \frac{\xi(k)}{2\sqrt{\xi(k)^2 + \Delta(k)^2}} = \frac{E(k) - \xi(k)}{2E(k)} \end{aligned} \quad (\text{B9})$$

which are the correlators in the ground state of a Kitaev chain. The entanglement entropy derived from this correlation matrix transitions between two distinct phases where the topologically non trivial phase $\gamma < \alpha$ is associated with a finite value of $S^{\text{top}} = 1$ while the trivial phase $\gamma > \alpha$ gives $S^{\text{top}} = 0$.

In the presence of a finite $w \neq 0$ the steady state solution is modified to:

$$\begin{aligned} F_k &= \frac{\sqrt{\rho(k)}}{2(1 + \rho(k))} \left(2i \sin \phi(k) - \sqrt{\rho(k)} + \frac{1}{\sqrt{\rho(k)}} \right) \\ C_k &= \frac{1}{2} - \frac{\sqrt{\rho(k)}}{2(1 + \rho(k))} \cos \phi(k) \end{aligned} \quad (\text{B10})$$

where

$$\rho(k) = \sqrt{\frac{\xi(k)^2 + (\Delta(k) - w(k))^2}{\xi(k)^2 + (\Delta(k) + w(k))^2}} \quad (\text{B11})$$

$$\tan \phi(k) = -\frac{2\Delta(k)\xi(k)}{\xi(k)^2 - \Delta(k)^2 + w(k)^2} \quad (\text{B12})$$

These equations correspond to the correlators in the ground state of the Kitaev chain with non-hermitian hopping.

We therefore establish that under post selected dynamics, the quantum state evolves to the dark state of the $\mathcal{H} = H_h - iH_{nh} = -i\mathcal{K}$. Here \mathcal{K} is the Hamiltonian of the Kitaev chain with non hermitian hopping, and the dark state of \mathcal{H} is identified with the ground state of \mathcal{K} . We describe below some features of this model. The corresponding BdG Hamiltonian is given by:

$$\begin{aligned} \mathcal{K}_{BdG} &= \begin{pmatrix} \xi(k) + iw(k) & -i\Delta(k) \\ i\Delta(k) & -\xi(k) - iw(k) \end{pmatrix} \\ &= (\xi(k) + iw(k)) \tau_z + \Delta(k) \tau_y \end{aligned} \quad (\text{B13})$$

Besides charge conjugation symmetry this model has chiral symmetry which can be made apparent by rotating to the chiral basis

$$\mathcal{K}_{BdG}^{\text{chiral}}(k) = \begin{pmatrix} 0 & q_1(k) \\ q_2(k) & 0 \end{pmatrix}, \quad (\text{B14})$$

where

$$q_{1,2}(k) = \xi(k) + i[w(k) \pm \Delta(k)] \quad (\text{B15})$$

In the hermitian limit $w = 0$ we have $q_1(k) = q_2(k)^*$ and the complex vector $q_1(k) = \gamma + \alpha e^{-ik}$ marks a circle of radius α centered around γ . In the non hermitian model the two complex vectors mark two tilted ellipses, similar to the non Hermitian SSH model [58, 70–73]. Gapped phases of this model are dichotomized by whether the two ellipses encapsulate the origin. The transition between these two distinct behaviors occurs when the two complex vectors pass through the origin and the spectrum becomes gapless. The condition for the onset of a gapless phase is $q_{1,2}(k) = 0$ which corresponds to:

$$\begin{aligned} \xi(k) &= 0 \\ \Delta(k) &= \pm w(k) \end{aligned} \quad (\text{B16})$$

Solving this set of equations, the transition to a gapless phase occurs for $\gamma = \frac{\alpha}{\sqrt{1+w^2/\alpha^2}}$. The phase diagram of the non Hermitian model exhibits three distinct phases. Two topologically distinct gapped phases, distinguished by the winding of both $\nu_{1,2} = 1$ or none $\nu_{1,2} = 0$ of the complex vectors $q_{1,2}(k)$, separated by a gapless phase, see Fig. 5.

-
- [1] R. Nandkishore and D. A. Huse, Many-body localization and thermalization in quantum statistical mechanics, *Annu. Rev. Condens. Matter Phys.* **6**, 15 (2015).
- [2] D. A. Abanin, E. Altman, I. Bloch, and M. Serbyn, Colloquium: Many-body localization, thermalization, and entanglement, *Reviews of Modern Physics* **91**, 021001 (2019).
- [3] J. Preskill, Quantum computing in the nisq era and beyond, *Quantum* **2**, 79 (2018).
- [4] J. Maldacena, S. H. Shenker, and D. Stanford, A bound on chaos, *Journal of High Energy Physics* **2016**, 1 (2016).
- [5] A. Kitaev, A simple model of quantum holography, <http://online.kitp.ucsb.edu/online/entangled15/kitaev/> (2015).
- [6] K. A. Landsman, C. Figgatt, T. Schuster, N. M. Linke, B. Yoshida, N. Y. Yao, and C. Monroe, Verified quantum information scrambling, *Nature* **567**, 61 (2019).
- [7] Y. Li, X. Chen, and M. P. A. Fisher, Quantum Zeno effect and the many-body entanglement transition, *Phys. Rev. B* **98**, 205136 (2018).
- [8] A. Chan, R. M. Nandkishore, M. Pretko, and G. Smith, Unitary-projective entanglement dynamics, *Phys. Rev. B* **99**, 224307 (2019).
- [9] B. Skinner, J. Ruhman, and A. Nahum, Measurement-induced phase transitions in the dynamics of entanglement, *Phys. Rev. X* **9**, 031009 (2019).
- [10] Y. Li, X. Chen, and M. P. A. Fisher, Measurement-driven entanglement transition in hybrid quantum circuits, *Phys. Rev. B* **100**, 134306 (2019).
- [11] M. Szytniszewski, A. Romito, and H. Schomerus, Entanglement transition from variable-strength weak measurements, *Phys. Rev. B* **100**, 064204 (2019).
- [12] S. Roy, J. T. Chalker, I. V. Gornyi, and Y. Gefen, Measurement-induced steering of quantum systems, *Phys. Rev. Research* **2**, 033347 (2020).
- [13] N. Lang and H. P. Büchler, Entanglement transition in the projective transverse field Ising model, *Phys. Rev. B* **102**, 094204 (2020).
- [14] A. Lavasani, Y. Alavirad, and M. Barkeshli, Measurement-induced topological entanglement transitions in symmetric random quantum circuits, *Nat. Phys.* **17**, 342 (2021).
- [15] A. Lavasani, Y. Alavirad, and M. Barkeshli, Topological order and criticality in (2+1)D monitored random quantum circuits, [arXiv:2011.06595](https://arxiv.org/abs/2011.06595) (2020).
- [16] M. Ippoliti, M. J. Gullans, S. Gopalakrishnan, D. A. Huse, and V. Khemani, Entanglement phase transitions in measurement-only dynamics, *Phys. Rev. X* **11**, 011030 (2021).
- [17] A. Kitaev and J. Preskill, Topological entanglement entropy, *Phys. Rev. Lett.* **96**, 110404 (2006).
- [18] M. Levin and X.-G. Wen, Detecting topological order in a ground state wave function, *Phys. Rev. Lett.* **96**, 110405 (2006).
- [19] J. R. Petta, A. C. Johnson, J. M. Taylor, E. A. Laird, A. Yacoby, M. D. Lukin, C. M. Marcus, M. P. Hanson, and A. C. Gossard, Coherent manipulation of coupled electron spins in semiconductor quantum dots, *Science* **309**, 2180 (2005).
- [20] D. Kim, Z. Shi, C. Simmons, D. Ward, J. Prance, T. S. Koh, J. K. Gamble, D. Savage, M. Lagally, M. Friesen, *et al.*, Quantum control and process tomography of a semiconductor quantum dot hybrid qubit, *Nature* **511**, 70 (2014).
- [21] A. West, B. Hensen, A. Jouan, T. Tanttu, C.-H. Yang, A. Rossi, M. F. Gonzalez-Zalba, F. Hudson, A. Morello, D. J. Reilly, *et al.*, Gate-based single-shot readout of spins in silicon, *Nat. Nanotechnol.* **14**, 437 (2019).

- [22] P. Maioli, T. Meunier, S. Gleyzes, A. Auffeves, G. Nogues, M. Brune, J. M. Raimond, and S. Haroche, Nondestructive Rydberg atom counting with mesoscopic fields in a cavity, *Phys. Rev. Lett.* **94**, 113601 (2005).
- [23] P. Neumann, J. Beck, M. Steiner, F. Rempp, H. Fedder, P. R. Hemmer, J. Wrachtrup, and F. Jelezko, Single-shot readout of a single nuclear spin, *Science* **329**, 542 (2010).
- [24] K. Murch, S. Weber, C. Macklin, and I. Siddiqi, Observing single quantum trajectories of a superconducting quantum bit, *Nature* **502**, 211 (2013).
- [25] M. Szyniszewski, A. Romito, and H. Schomerus, Universality of entanglement transitions from stroboscopic to continuous measurements, *Phys. Rev. Lett.* **125**, 210602 (2020).
- [26] X. Turkeshi, A. Biella, R. Fazio, M. Dalmonte, and M. Schiró, Measurement-induced entanglement transitions in the quantum Ising chain: From infinite to zero clicks, *Phys. Rev. B* **103**, 224210 (2021).
- [27] Q. Tang and W. Zhu, Measurement-induced phase transition: A case study in the nonintegrable model by density-matrix renormalization group calculations, *Phys. Rev. Research* **2**, 013022 (2020).
- [28] S. Goto and I. Danshita, Measurement-induced transitions of the entanglement scaling law in ultracold gases with controllable dissipation, *Phys. Rev. A* **102**, 033316 (2020).
- [29] Y. Fuji and Y. Ashida, Measurement-induced quantum criticality under continuous monitoring, *Phys. Rev. B* **102**, 054302 (2020).
- [30] D. Rossini and E. Vicari, Measurement-induced dynamics of many-body systems at quantum criticality, *Phys. Rev. B* **102**, 035119 (2020).
- [31] D. Rossini and E. Vicari, Coherent and dissipative dynamics at quantum phase transitions, arXiv:2103.02626 (2021).
- [32] O. Lunt and A. Pal, Measurement-induced entanglement transitions in many-body localized systems, *Phys. Rev. Research* **2**, 043072 (2020).
- [33] T. Boorman, M. Szyniszewski, H. Schomerus, and A. Romito, Diagnosing entanglement dynamics in noisy and disordered spin chains via the measurement-induced steady-state entanglement transition, arXiv preprint arXiv:2107.11354 (2021).
- [34] X. Chen, Y. Li, M. P. A. Fisher, and A. Lucas, Emergent conformal symmetry in nonunitary random dynamics of free fermions, *Phys. Rev. Research* **2**, 033017 (2020).
- [35] C. Liu, P. Zhang, and X. Chen, Non-unitary dynamics of Sachdev-Ye-Kitaev chain, *SciPost Phys.* **10**, 48 (2021).
- [36] A. Biella and M. Schiró, Many-body quantum zeno effect and measurement-induced subradiance transition, arXiv:2011.11620 (2020).
- [37] S. Gopalakrishnan and M. J. Gullans, Entanglement and purification transitions in non-Hermitian quantum mechanics, *Phys. Rev. Lett.* **126**, 170503 (2021).
- [38] S.-K. Jian, Z.-C. Yang, Z. Bi, and X. Chen, Yang-Lee edge singularity triggered entanglement transition, arXiv:2101.04115 (2021).
- [39] Q. Tang, X. Chen, and W. Zhu, Quantum criticality in the nonunitary dynamics of $(2+1)$ -dimensional free fermions, *Phys. Rev. B* **103**, 174303 (2021).
- [40] X. Turkeshi, Measurement-induced criticality as a data-structure transition, arXiv:2101.06245 (2021).
- [41] X. Turkeshi, M. Dalmonte, R. Fazio, and M. Schiró, Entanglement transitions from stochastic resetting of non-hermitian quasiparticles, arXiv preprint arXiv:2111.03500 (2021).
- [42] A. Altland, M. Buchhold, S. Diehl, and T. Micklitz, Dynamics of measured many-body quantum chaotic systems, arXiv preprint arXiv:2112.08373 (2021).
- [43] Y. Minoguchi, P. Rabl, and M. Buchhold, Continuous gaussian measurements of the free boson cft: A model for exactly solvable and detectable measurement-induced dynamics, *SciPost Physics* **12**, 009 (2022).
- [44] X. Cao, A. Tilloy, and A. D. Luca, Entanglement in a fermion chain under continuous monitoring, *SciPost Phys.* **7**, 24 (2019).
- [45] O. Alberton, M. Buchhold, and S. Diehl, Entanglement transition in a monitored free-fermion chain: From extended criticality to area law, *Phys. Rev. Lett.* **126**, 170602 (2021).
- [46] T. Müller, S. Diehl, and M. Buchhold, Measurement-induced dark state phase transitions in long-ranged fermion systems, *Physical Review Letters* **128**, 010605 (2022).
- [47] M. Buchhold, Y. Minoguchi, A. Altland, and S. Diehl, Effective theory for the measurement-induced phase transition of Dirac fermions, arXiv:2102.08381 (2021).
- [48] K. Jacobs, *Quantum measurement theory and its applications* (Cambridge University Press, 2014).
- [49] Note that, under the Jordan-Wigner transformation, the measurements of M_j and \tilde{M}_j are mapped to measurements of $S_{z,j}$ and $S_{x,j}S_{x,j+1}$, respectively.
- [50] A. Y. Kitaev, Unpaired majorana fermions in quantum wires, *Physics-uspekhi* **44**, 131 (2001).
- [51] M. Van Regemortel, Z.-P. Cian, A. Seif, H. Dehghani, and M. Hafezi, Entanglement entropy scaling transition under competing monitoring protocols, *Physical Review Letters* **126**, 123604 (2021).
- [52] B. Zeng and X.-G. Wen, Gapped quantum liquids and topological order, stochastic local transformations and emergence of unitarity, *Phys. Rev. B* **91**, 125121 (2015).
- [53] B. Zeng and D. L. Zhou, Topological and error-correcting properties for symmetry-protected topological order, *EPL (Europhysics Letters)* **113**, 56001 (2016).
- [54] I. Peschel, Calculation of reduced density matrices from correlation functions, *Journal of Physics A: Mathematical and General* **36**, L205 (2003).
- [55] S. Nulty, J. Vala, D. Meidan, and G. Kells, Constrained thermalization and topological superconductivity, *Phys. Rev. B* **102**, 054508 (2020).

- [56] H. M. Wiseman and G. J. Milburn, *Quantum Measurement and Control* (Cambridge University Press, 2009).
- [57] M. S. Rudner and L. Levitov, Topological transition in a non-hermitian quantum walk, *Physical review letters* **102**, 065703 (2009).
- [58] L. Herviou, J. H. Bardarson, and N. Regnault, Defining a bulk-edge correspondence for non-hermitian hamiltonians via singular-value decomposition, *Phys. Rev. A* **99**, 052118 (2019).
- [59] A. C. Johnson, J. Petta, C. Marcus, M. Hanson, and A. Gossard, Singlet-triplet spin blockade and charge sensing in a few-electron double quantum dot, *Physical Review B* **72**, 165308 (2005).
- [60] D. Reilly, C. Marcus, M. Hanson, and A. Gossard, Fast single-charge sensing with a rf quantum point contact, *Applied Physics Letters* **91**, 162101 (2007).
- [61] Z. Liu, E. J. Bergholtz, A. Romito, and D. Meidan, Interacting majorana chain: Transport properties and signatures of an emergent two-dimensional weak topological phase, *Phys. Rev. B* **96**, 205442 (2017).
- [62] A. Romito and Y. Gefen, Ubiquitous nonlocal entanglement with majorana zero modes, *Physical review letters* **119**, 157702 (2017).
- [63] J. F. Steiner and F. von Oppen, Readout of majorana qubits, *Physical Review Research* **2**, 033255 (2020).
- [64] M. I. Munk, J. Schulenburg, R. Egger, and K. Flensberg, Parity-to-charge conversion in majorana qubit readout, *Physical Review Research* **2**, 033254 (2020).
- [65] J. Manousakis, C. Wille, A. Altland, R. Egger, K. Flensberg, and F. Hassler, Weak measurement protocols for majorana bound state identification, *Physical review letters* **124**, 096801 (2020).
- [66] L. Fu, Electron teleportation via majorana bound states in a mesoscopic superconductor, *Phys. Rev. Lett.* **104**, 056402 (2010).
- [67] B. Béri and N. R. Cooper, Topological kondo effect with majorana fermions, *Phys. Rev. Lett.* **109**, 156803 (2012).
- [68] B. Béri, Majorana-klein hybridization in topological superconductor junctions, *Phys. Rev. Lett.* **110**, 216803 (2013).
- [69] A. Altland and R. Egger, Multiterminal coulomb-majorana junction, *Phys. Rev. Lett.* **110**, 196401 (2013).
- [70] Z. Gong, Y. Ashida, K. Kawabata, K. Takasan, S. Higashikawa, and M. Ueda, Topological phases of non-hermitian systems, *Phys. Rev. X* **8**, 031079 (2018).
- [71] K. Kawabata, K. Shiozaki, M. Ueda, and M. Sato, Symmetry and topology in non-hermitian physics, *Phys. Rev. X* **9**, 041015 (2019).
- [72] F. K. Kunst, E. Edvardsson, J. C. Budich, and E. J. Bergholtz, Biorthogonal bulk-boundary correspondence in non-hermitian systems, *Phys. Rev. Lett.* **121**, 026808 (2018).
- [73] S. Lieu, Topological phases in the non-hermitian su-schrieffer-heeger model, *Phys. Rev. B* **97**, 045106 (2018).